Unified model of brain tissue microstructure dynamically binds diffusion and osmosis with extracellular space geometry

Mohsen Yousefnezhad,[1,*] Morteza Fotouhi,[1] Kaveh Vejdani,[2] and Padideh Kamali-Zare[3]

[1]*Department of Mathematical Sciences, Sharif University of Technology, Tehran 11365-9415, Iran*
[2]*Department of Nuclear Medicine, Stanford Healthcare, Palo Alto, California 94304, USA*
[3]*Department of Physiology & Neuroscience, New York University, School of Medicine, New York, New York 10016, USA*

We present a universal model of brain tissue microstructure that dynamically links osmosis and diffusion with geometrical parameters of brain extracellular space (ECS). Our model robustly describes and predicts the nonlinear time dependency of tortuosity ($\lambda = \sqrt{D/D^*}$) changes with very high precision in various media with uniform and nonuniform osmolarity distribution, as demonstrated by previously published experimental data (D = free diffusion coefficient, D^* = effective diffusion coefficient). To construct this model, we first developed a multiscale technique for computationally effective modeling of osmolarity in the brain tissue. Osmolarity differences across cell membranes lead to changes in the ECS dynamics. The evolution of the underlying dynamics is then captured by a level set method. Subsequently, using a homogenization technique, we derived a coarse-grained model with parameters that are explicitly related to the geometry of cells and their associated ECS. Our modeling results in very accurate analytical approximation of tortuosity based on time, space, osmolarity differences across cell membranes, and water permeability of cell membranes. Our model provides a unique platform for studying ECS dynamics not only in physiologic conditions such as sleep-wake cycles and aging but also in pathologic conditions such as stroke, seizure, and neoplasia, as well as in predictive pharmacokinetic modeling such as predicting medication biodistribution and efficacy and novel biomolecule development and testing.

I. INTRODUCTION

Recent advances in the understanding of a variety of brain diseases has led to the identification of molecular, genetic, and epigenetic mechanisms underlying physiological and pathological processes at microscopic and macroscopic levels. Many of these disorders in the brain are accompanied by a disruption in water and solute balance in the central nervous system (CNS). This imbalance leads to changes in both intra- and extracellular compartments of the tissue. Almost 80% of the brain tissue is within the intracellular space (ICS) and approximately 20% in the extracellular space (ECS). The ICS is interconnected only through synapses and gap junctions, which are mainly involved in neuronal signal transmission, which is outside the scope of this paper. The ECS, on the other hand, is a globally interconnected space throughout the brain, which forms a microenvironment for cells in which water and biomolecules diffuse, distribute, and produce effects. Therefore, variation in the size and geometry of the ECS can be important for the local modulation of molecular transport and water and solute homeostasis in the brain.

Molecular diffusion in the brain ECS plays a critical role in fundamental biological processes such as the movement of metabolic substrates and volume transmission [1]. Volume transmission is also known as extrasynaptic or nonsynaptic transmission and has been proposed to be another mechanism

for intercellular communication via substance diffusion in the ECS [2–4]. Understanding the basics of ECS has already found important clinical applications such as diffusion-weighted magnetic resonance imaging [5,6] and drug delivery [7,8]. Any change in the parameters that influence the diffusion process within the ECS can substantially affect neuronal signal transmission. Two major structural parameters that characterize the diffusion properties of the ECS are tortuosity (λ) and volume fraction (α) [9–12]. Tortuosity quantifies the hindrance imposed on the diffusion process by the tissue, as compared with water. Tortuosity is defined as $\lambda = \sqrt{D/D^*}$, where D is the free diffusion coefficient and D^* is the effective diffusion coefficient in the brain [9–12]. Volume fraction is simply the proportion of the tissue volume occupied by the ECS. It is calculated as $\alpha = V_{\text{ECS}}/V_{\text{Tissue}}$, where V_{ECS} and V_{Tissue} are the volumes of ECS and the whole tissue, respectively. To increase our understanding of the cellular response to physiological and pathological conditions, such as the prediction and early detection of acute cerebral ischemia, these parameters have been extensively studied and quantified in the brain tissue. There have been many attempts to compute tortuosity from models representing the brain's geometrical structure [13–16].

Brain ECS diffusion parameters are not constant. Through extrasynaptic transmission, almost all pathologic and physiologic changes of the CNS state lead to considerable changes in the ECS diffusion properties. The nature of the evoking stimulus determines not only the way in which the ECS size and tortuosity change but also how rapidly these changes occur. Acute pathological states such as ischemia and CNS injury are accompanied by dramatic cell swelling leading to ECS shrinkage of about 60–75% (α reducing to 0.05) [17]. Diffusion in the ECS is affected by cell (especially glial)

---

*Corresponding author: yousefnezhad@mehr.sharif.ir; mohsen.yousefnezhad@gmail.com. Please address reprint requests to Mohsen Yousefnezhad, Department of Mathematical Sciences, Sharif University of Technology, Azadi Ave., Tehran, Iran.

swelling, resulting from water shifts between intra- and extracellular compartments [17–19].

Water transport across cellular membranes in the brain is thought to be mainly regulated by astrocytic end-feet aquaporin (AQP4) channels [20,21]. Aquaporins are water-selective channels ubiquitous in the living world [22,23]. Since their discovery in 1992, members of the AQP family have been described in all living organisms [24,25] and efforts to further understand their regulation has given rise to a wide range of discoveries [26,27]. Water movement in the brain is likely to involve AQP4 channels, which are widely expressed in astrocytes and other glial cells [20] and possess the highest water permeability among all members of the AQP family. Interestingly, the brain is the only major organ other than the lungs and kidneys where AQP4 is abundantly expressed. As such, AQP4 and its regulators could be potential targets for the treatment of brain disorders involving disturbances in water homeostasis [25]. Inhibition of AQP4 may provide therapeutic options for preventing cerebral edema in stroke and water intoxication [28–30]. We have implemented the high-permeability characteristic of AQP4 in our model, as will be described further below.

The mechanistic link between diffusion parameters in the brain ECS, osmosis, and membrane water permeability has been unclear in the literature. In recent years, mathematical models and computational methods have been increasingly used to support or disprove various proposed scenarios of nonlinear dynamic changes of ECS geometry under various physiological and pathological conditions, as well as to provide a context for the interpretation of experimental findings. In the process, new models have been designed and new paradigms for interpreting model predictions have been formulated. To our knowledge, none of these models successfully links ECS size and tortuosity with osmosis and membrane permeability to accurately describe or predict the nonlinear time dependency of ECS dynamics under various conditions.

The present study provides a detailed understanding of the major parameters that determine water balance and solute diffusion in the brain. We show how the time course of changes in these parameters is affected by cell membrane permeability and osmolarity gradients between ECS and ICS. Since the motion of solute particles in the ECS takes place in a multiscale environment [9], we have constructed a multiscale mathematical model which describes the dynamic relation between osmotic gradient, cell membrane water permeability, ECS volume fraction, and ECS tortuosity. A unique aspect and technical challenge of our model was the modeling of diffusion for a nonstationary ICS-ECS interface in the brain tissue with the assumption that the cell membrane is highly permeable to water. This assumption is supported by the known abundance of AQP4 channels in glial cell membranes. A strength of our model is that it formulates osmolarity-driven diffusion in ECS and ICS with minimal parameters.

In the sections that follow, we first provide a detailed description of the presented mathematical model. This starts with a description of a scalable representative tissue geometry. A level set equation is then used to describe the membrane interface as a moving boundary and to describe the dynamics of ECS changes driven by osmolarity gradients. A homogenization technique is then used in the framework of this level set

method to derive a spatially averaged diffusion model. This involves asymptotic expansion of the spatial gradient functions, followed by solutions to the lowest-order problems, reference cell problems, and homogenized problems. Afterwards, the dynamics of the ECS and ICS osmolarities are scaled up to provide a macroscopic description of transport processes. An explicit derivation of the tortuosity factor as a function of the relevant parameters—time, space, ECS diffusivity, osmolarity difference across the cell membrane, and cell membrane water permeability—completes the presented mathematical model.

Second, we present multiple realistic examples, with numerical schemes for simulation of the theoretical results to demonstrate how ECS tortuosity is related to the dynamic size of the ECS, time, space, membrane water permeability, and osmolarity gradient across cell membranes. These examples start with a representation of tortuosity as a function of ECS volume fraction. Afterwards, we demonstrate the time evolution of tortuosity and volume fraction for multiple values of osmolarity difference across cell membrane and separately again for multiple values of membrane water permeability. Next, the case of nonuniform osmolarity distribution is studied, and simulated results of the time evolution of tortuosity are presented for four discrete points in space. A thorough demonstration of time-concentration profiles for microscale (nonhomogenized) and homogenized models in both uniform and nonuniform osmolarity distribution cases completes the set of simulated examples. Finally, a detailed discussion and brief conclusion are presented in the last section.

II. MATHEMATICAL MODEL

In this section, we provide a two-dimensional (2D) multi-scale mathematical model of osmolarity evolutions in brain ECS and ICS. The mathematical model presented here is designed for brain tissue experiencing dynamic ECS changes. In this study, the ICS and ECS are modelled as perfectly mixed phases separated by an ideal semipermeable membrane with a vanishingly small elastic modulus. ECS changes are caused by osmotic effects that lead to water transport through cellular membranes. In our problem layout we assume that at time zero the osmolarity of the ECS is less than the osmolarity of the ICS, resulting in water transport from outside of the cells to inside the cells. This leads to swelling of the cells and shrinkage of the ECS. The correlation between ECS volume fraction (α) and tortuosity (λ) with osmotic challenge has been the subject of several theoretical studies in two dimensions [13] and some experimental studies [31].

The current model is described as a moving boundary problem in which two phases containing diffusive osmolytes are separated by a weakly elastic and ideally semipermeable membrane. The water flux across the cell membrane is linearly dependent on the osmolarity difference across the membrane.

A. Setting

Diffusion in the ECS is controlled by its geometry and content and is analogous to diffusion in porous media with several scales [9,32]. The system is characterized by a clear separation of length scales: The size of a single cell including the narrow gap between cells is several microns, whereas the dimension
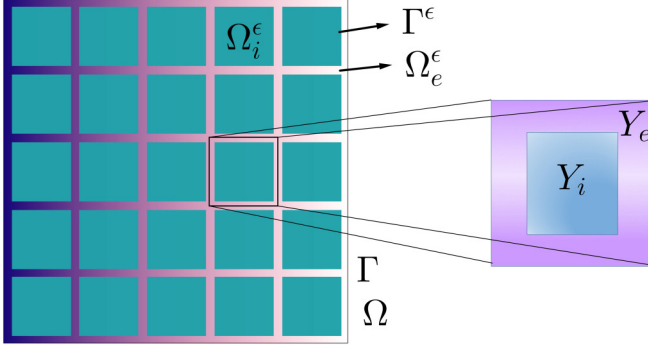
FIG. 1. Schematic illustration of the geometrical setting used in the multiscale mathematical model under homogenization procedure.

of the brain tissue block is in the order of hundreds of microns. We introduce the small scale parameter ϵ as the ratio of the size of the pore (l) to the size of our selected tissue (L):

$$\epsilon = \frac{l}{L}.$$

First, for the geometry of a selected tissue, we consider a rectangular region Ω with boundary Γ, as a selected region in the brain tissue with a periodic repetition of an ϵ-scaled reference cell (ϵY), where Y is the reference element and contains a single cell (Y^i) together with its associated extracellular region (Y^e), where, $\bar{Y}_i \cup \bar{Y}_e = \bar{Y}$ ($\bar{Y}$ is the closure Y), $\bar{Y}_i \cap \bar{Y}_e =: \Gamma$, $Y_i \cap Y_e = \emptyset$ and ϵ is a small, dimensionless length scale. In this periodic geometry Ω_i^ϵ represents ICS, Γ^ϵ is the membrane of the cells, and Ω_e^ϵ is the associated ECS (Fig. 1). Such periodic distribution of cells, although not realistic, is sufficient to show significant effects of water transport on molecular diffusion in the brain, as demonstrated below.

B. Membrane interface

In order to describe the evolution of the underlying microstructure induced by cell swelling, we define the level set function G at time (t) and space (x) variable by:

$$G(x,t) \begin{cases} < 0 & \text{extracellular space} \\ = 0 & \text{membrane} \\ > 0 & \text{intracellular space} \end{cases}.$$

A level set function is an appropriate tool for studying moving interfaces and has inspired new ways of numerically solving moving boundary problems [33,34]. Here we assume that there is no tangential movement of the membrane. Fulfilling the following partial differential equation:

$$\begin{aligned} G_t + v_n |\nabla G| = 0 \quad & t \in (0,T), x \in \Omega, \\ G(x,0) = S_0, \end{aligned} \tag{1}$$

where v_n is the normal velocity of the membrane interface (will be determined later). Also, the evolving membrane is defined by $\Gamma(t) = \{x : G(x,t) = 0\}$, the ECS is given by $\Omega_e(t) = \{x : G(x,t) < 0\}$, and the ICS is given by $\Omega_i(t) = \{x : G(x,t) > 0\}$.

C. Mathematical formulation

In this study, we assume that there is no advective component in the basic equation for osmolyte diffusion. In other words, there is no global fluid movement in the model. The only motion considered in the model is cell membrane translation in a medium of zero net velocity. This constitutes a moving boundary problem.

Substances that are released into the ECS move predominantly by diffusion [10,11]. Thus, the evolution of osmolarity concentration due to diffusion in the porous extracellular space is given by the following set of partial differential equations:

$$\partial_t \psi - \nabla.(D_e \nabla \psi) = 0 \quad t \in (0,T), x \in \Omega_e(t), \tag{2}$$

with homogeneous diffusivity D_e and osmolarity of ECS, ψ.

Similarly, the evolution of osmolarity due to diffusion in the intracellular space is given by the following set of partial differential equations:

$$\partial_t \phi - \nabla.(D_i \nabla \phi) = 0 \quad t \in (0,T), x \in \Omega_i(t), \tag{3}$$

with homogeneous diffusivity D_i and osmolarity of ICS, ϕ.

A crucial point in this formulation is the derivation of appropriate boundary conditions at the ECS-ICS interface. Now we derive boundary conditions at the moving interface for concentrations. The plasma membrane separates the intracellular and extracellular compartments. In the time scale of water flux in most cells, solute fluxes between these compartments are slow relative to water fluxes [35]. Thus, if a change is made to the extracellular solute concentration, water will redistribute quickly, maintaining equal osmolarities in both compartments [35]. So, for simplicity, we consider that the membrane interface is impermeable to solutes.

Despite the semipermeable nature of cell membranes, the cell membrane in our model is assumed to be permeable to water only, because this provides a case where we can study the effect of water transport (in extreme cases) on the geometrical characteristics of the ECS (e.g., tortuosity) without the influence of any other parameter associated with membrane transport.

The starting condition in our model is an initial osmotic imbalance that is assumed to be dissipated only by water transport and not solute transport through the membrane. In order to derive physically meaningful boundary conditions, a conservation law at the evolving interface is required. In fact, the Rankine-Hugoniot condition guarantees conservation of quantities across a moving boundary [36]. The Rankine-Hugoniot condition for conserving ECS osmolarity across the moving interface is as follows:

$$D_i \nabla \phi(x,t) \cdot \mathbf{n} + v_n(x,t)\phi(x,t) = 0, \tag{4}$$

where $\mathbf{n}$ is unit normal pointing into the ICS and v_n is the normal velocity of the membrane. This condition gives us a relationship between the preserved concentrations and their fluxes across the moving boundary, hence giving boundary conditions that are useful for our purpose.

The ICS swelling and ECS shrinkage leads to the membrane interface moving from ICS to ECS. One crucial physical factor related to the ECS geometry is the ECS size, which is relatively small compared to the ICS compartment. As a result of such a big volume difference, the ECS experiences a higher change in

its initial osmolarity during the course of water transport from the ECS to ICS in response to the osmotic challenge. This is reflected in our boundary condition.

Details of the derivation of the boundary condition are given in the Appendix.

The relative velocity of the membrane with respect to fluid is directly proportional to the difference between the ICS and ECS osmolarities [37,38]:

$$v_n(x,t) = p_f v_w(\psi - \phi), \tag{5}$$

where p_f is the cell membrane water permeability and v_w is partial molar volume of water. In this study, we assume that water permeability is constant across all parts of the cell membrane.

D. Homogenization

Our model belongs to the class of spatially periodic heterogeneous materials that can be studied by a technique called homogenization. The formal approach of homogenization theory, namely the method of asymptotic expansions, has been widely used to study a variety of processes in physics, engineering, and biology [39–44]. The main theoretical issue is that if one draws a line through a selected brain tissue (Fig. 2) and measures the extracellular concentration of molecules along that line, the concentrations are spatially heterogeneous.

By using some types of averaging that, on an appropriate length scale, smooth out the heterogeneities, we can simplify the problem and make it solvable with numerical techniques. The main goal of homogenization is to do such averaging over the substructural variations in materials that are spatially heterogeneous (Fig. 2). Homogenization theory relies on the assumption that the medium is composed of the spatial repetition of much smaller reference cells [40].

(a)

(b)

(c)
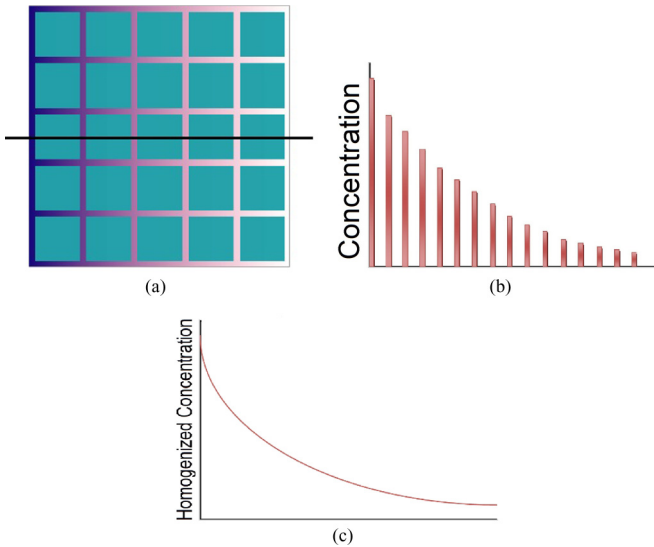
FIG. 2. Geometric model of the brain tissue. Depictive example showing that the method of homogenization effectively smooths substructure variations caused by brain spatial heterogenetics. A cross section in the medium alternately intersects the two phases (a). A cross section of the solution at a given time in ECS (b) is compared to the solution of the homogenized equation (c).

Here, first, a microscopic description of the phenomenon is established in the reference cell. The asymptotic expansion technique is then employed to derive a simplified macroscopic problem for the entire domain, with coefficients that are dependent on the microscopic properties. In this study, to describe the ECS volume changes due to osmosis, we use homogenization technique in the framework of the level set method. Separation of length scales is the basis of homogenization technique. We introduce the small scale parameter ϵ as the ratio of the size of the pore (l) to the size of our selected tissue (L):

$$\epsilon = \frac{l}{L}. \tag{6}$$

For our purpose, we reformulate the equations within the multiscale framework. In order to obtain process-adapted models in the homogenization limit, it is important to identify the characteristic microscopic and macroscopic lengths and to properly nondimensionalize the system of equations [45,46].

Reasonable scaling can be derived, for example, by performing a nondimensionalization procedure, which reveals the weighting of the different processes. In order to nondimensionalize the problem, we define the following dimensionless variables:

$$\tilde{x} = x/L, \quad \tilde{t} = t/t_{\mathrm{ref}}, \quad \tilde{\psi}_\epsilon = \psi_\epsilon/\psi_{\mathrm{ref}},$$
$$\tilde{\phi}_\epsilon = \phi_\epsilon/\psi_{\mathrm{ref}} \quad \tilde{G} = G/l,$$

and dimensionless parameters:

$$\tilde{D}_e^\epsilon = \frac{t_{\mathrm{ref}}}{L^2}D_e^\epsilon, \quad \tilde{D}_i^\epsilon = \frac{t_{\mathrm{ref}}}{L^2}D_i^\epsilon, \quad \tilde{p}_f = \frac{t_{\mathrm{ref}}}{l}p_f, \quad \tilde{v}_w = \psi_{\mathrm{ref}}v_w,$$

where ψ_{ref} and t_{ref} are a reference concentration and a reference time, respectively.

From (1), (2), (3), (4), (5), and (6), the following dimensionless model is obtained:

$$\begin{aligned}
\partial_{\tilde{t}}\tilde{\psi}_\epsilon &= \tilde{\nabla} \cdot (\tilde{D}_e \tilde{\nabla} \tilde{\psi}_\epsilon) & \tilde{x} \in \tilde{\Omega}_e^\epsilon(t), \tilde{t} \in (0, \tilde{T}) \\
\partial_{\tilde{t}}\tilde{\phi}_\epsilon &= \tilde{\nabla} \cdot (\tilde{D}_i \tilde{\nabla} \tilde{\phi}_\epsilon) & \tilde{x} \in \tilde{\Omega}_i^\epsilon(t), \tilde{t} \in (0, \tilde{T}) \\
\partial_{\tilde{t}}\tilde{G}_\epsilon + \epsilon \tilde{v}_n |\tilde{\nabla} \tilde{G}_\epsilon| &= 0 & \tilde{x} \in \tilde{\Omega}, \tilde{t} \in (0, \tilde{T}) \\
\tilde{D}_e \tilde{\nabla} \tilde{\psi}_\epsilon \cdot \mathbf{n}^\epsilon + \epsilon \tilde{v}_n \tilde{\psi}_\epsilon &= 0 & \tilde{x} \in \tilde{\Gamma}^\epsilon(t), \tilde{t} \in (0, \tilde{T}) \\
\tilde{D}_i \tilde{\nabla} \tilde{\phi}_\epsilon \cdot \mathbf{n}^\epsilon - \epsilon \tilde{v}_n \tilde{\phi}_\epsilon &= 0 & \tilde{x} \in \tilde{\Gamma}^\epsilon(t), \tilde{t} \in (0, \tilde{T}),
\end{aligned} \tag{7}$$

where

$$\tilde{v}_n = \tilde{p}_f \tilde{v}_w (\tilde{\psi} - \tilde{\phi}), \quad \tilde{x} \in \tilde{\Gamma}^\epsilon(t), \tilde{t} \in (0, \tilde{T}). \tag{8}$$

Subsequently, we describe the approach for deriving an equivalent macroscopic description from the dimensionless microscopic system (7). For more details about the homogenization technique, see Ref. [40]. In the following sections, tildes are omitted for convenience.

1. Asymptotic expansion

Brain tissue structure is considered a multiscale system; we characterize it by two spatial variables: the global variable x (slow variable) and a microscopic variable y (fast variable). Both are connected via the relation $y = x/\epsilon$. As a consequence, the expansion of the spatial gradient reads [40]:

$$\nabla = \nabla_x + \frac{1}{\epsilon}\nabla_y. $$

Higher-order spatial derivatives are calculated in a similar way by applying the chain rule.

Furthermore, the two-scale asymptotic expansions for all variable functions have the following form [40]:

$$\psi_\epsilon(x,t) = \psi_0(x,y,t) + \epsilon\psi_1(x,y,t) + \epsilon^2\psi_2(x,y,t) + \cdots,$$
$$\phi_\epsilon(x,t) = \phi_0(x,y,t) + \epsilon\phi_1(x,y,t) + \epsilon^2\phi_2(x,y,t) + \cdots,$$
$$(9)$$

where each term $\phi_k(x,y,t), \psi_k(x,y,t)$ is Y-periodic with respect to the microscopic variable.

In our work, we perform the homogenization procedure by handling the evolving microstructure directly by a level set function. This was first suggested in Ref. [47] in the framework of precipitation/dissolution reactions in porous media. In addition to the expansions (9), in the framework of a level set description, the level set function G_ϵ itself and the normal vector $\mathbf{n}_\epsilon$ are also expanded in terms of ϵ due to the evolving microstructure.

For a two-dimensional setting, the expansion of the normal vector is expressed by expansion of the level set function, and

we obtain the following expressions [47]:

$$G^\epsilon(x,t) = G_0(x,y,t) + \epsilon G_1(x,y,t) + \epsilon^2 G_2(x,y,t) + \cdots,$$
$$(10)$$

$$\mathbf{n}^\epsilon = \mathbf{n}_0 + \epsilon\mathbf{n}_1 + O(\epsilon^2), \quad \mathbf{n}_0 = \frac{\nabla_y G_0}{|\nabla_y G_0|},$$

$$\mathbf{n}_1 = \tau_0 \frac{\tau_0 \cdot (\nabla_x G_0 + \nabla_y G_1)}{|\nabla_y S_0|}, \qquad (11)$$

with $\tau_0 := \mathbf{n}_0^\perp$ denoting the orthogonal complement of $\mathbf{n}_0$ in the two-dimensional space.

The zero-order expansion of the level set function is also used to describe the zero-order time evolving domain $Y_0^e(x,t) = \{y : G_0(x,y,t) < 0\}$, $Y_0^i(x,t) = \{y : G_0(x,y,t) > 0\}$ and interface $\Gamma_0(x,t) = \{y : G_0(x,y,t) = 0\}$ [47]:

$$\partial_t G_0 + p_f v_w(\psi_0 - \phi_0)|\nabla_y G_0| = 0. \qquad (12)$$

For formal homogenization, the microscale is rewritten in terms of the asymptotic expansions. Then, by comparing the coefficient of different powers of ϵ, a cascade of equations for the terms $\phi_k(x,y,t)$ and $\psi_k(x,y,t)$ are obtained:

$$\partial_t \phi_0 = \frac{1}{\epsilon^2}\nabla_y^2\phi_0 + \frac{1}{\epsilon}\left(\nabla_x \cdot \nabla_y\phi_0 + \nabla_y \cdot \nabla_x\phi_0 + \nabla_y^2\phi_1\right) + \left(\nabla_x^2\phi_0 + \nabla_y^2\phi_2 + \nabla_x \cdot \nabla_y\phi_1 + \nabla_y \cdot \nabla_x\phi_1\right) + \epsilon(\cdots) \quad (13)$$

and, in a similar way,

$$\partial_t \psi_0 = \frac{1}{\epsilon^2}\nabla_y^2\psi_0 + \frac{1}{\epsilon}\left(\nabla_x \cdot \nabla_y\psi_0 + \nabla_y \cdot \nabla_x\psi_0 + \nabla_y^2\psi_1\right) + \left(\nabla_x^2\psi_0 + \nabla_y^2\psi_2 + \nabla_x \cdot \nabla_y\psi_1 + \nabla_y \cdot \nabla_x\psi_1\right) + \epsilon(\cdots). \quad (14)$$

Now we expand the boundary conditions:

$$D_i\nabla\phi_\epsilon \cdot \mathbf{n}^\epsilon + \epsilon v_n\phi_\epsilon = 0 \qquad (15)$$

by assigning ϕ_ϵ and $\mathbf{n}_\epsilon$ in (15), we will have:

$$D_i\left[\left(\nabla_x + \frac{1}{\epsilon}\nabla_y\right)\phi_0 + \epsilon\left(\nabla_x + \frac{1}{\epsilon}\nabla_y\right)\phi_1 + \epsilon^2\left(\nabla_x + \frac{1}{\epsilon}\nabla_y\right)\phi_2 + \cdots\right] \cdot (\mathbf{n}_0 + \epsilon\mathbf{n}_1 + \epsilon^2\mathbf{n}_2 + \cdots) + \epsilon v_n(\phi_0 + \epsilon\phi_1 + \cdots) = 0,$$

$$D_i\left[\frac{1}{\epsilon}\nabla_y\phi_0 + (\nabla_x\phi_0 + \nabla_y\phi_1) + \epsilon(\nabla_x\phi_1 + \nabla_y\phi_2) + \epsilon^2(\cdots)\right] \cdot (\mathbf{n}_0 + \epsilon\mathbf{n}_1 + \epsilon^2\mathbf{n}_2 + \cdots) + \epsilon v_n(\phi_0 + \epsilon\phi_1 + \cdots) = 0,$$

$$\frac{1}{\epsilon}D_i\nabla_y\phi_0 \cdot \mathbf{n}_0 + D_i\nabla_y\phi_0 \cdot \mathbf{n}_1 + D_i(\nabla_x\phi_0 + \nabla_y\phi_1) \cdot \mathbf{n}_0$$

$$+\epsilon[D_i\nabla_y\phi_0 \cdot \mathbf{n}_2 + D_i\nabla_x\phi_0 \cdot \mathbf{n}_1 + D_i\nabla_y\phi_1 \cdot \mathbf{n}_1 + D_i\nabla_x\phi_1 \cdot \mathbf{n}_0 + D_i\nabla_y\phi_2 \cdot \mathbf{n}_0 + p_f v_w(\psi_0 - \phi_0)\phi_0] + \epsilon^2(\cdots) = 0, \quad x \in \Gamma^\epsilon(t).$$

As in Ref. [47], for the formulation of upscaled model it would be convenient to have a boundary condition enforced at $\Gamma_0(x,t) = \{y : G_0(x,y,t) = 0\}$:

$$\frac{1}{\epsilon}D_i\nabla_y\phi_0 \cdot \mathbf{n}_0 + D_i\nabla_y\phi_0 \cdot \mathbf{n}_1 + D_i\nabla_x\phi_0 \cdot \mathbf{n}_0 + D_i\nabla_y\phi_1 \cdot \mathbf{n}_0 + y \cdot \nabla_x(D_i\nabla_y\phi_0 \cdot \mathbf{n}_0) + \lambda\mathbf{n}_0 \cdot \nabla_y(D_i\nabla_y\phi_0 \cdot \mathbf{n}_0)$$

$$+\epsilon\Big[y \cdot \nabla_x(D_i\nabla_y\phi_0 \cdot \mathbf{n}_1 + D_i\nabla_x\phi_0 \cdot \mathbf{n}_0 + D_i\nabla_y\phi_1 \cdot \mathbf{n}_0) + \lambda\mathbf{n}_0 \cdot \nabla_y(D_i\nabla_y\phi_0 \cdot \mathbf{n}_1 + D_i\nabla_x\phi_0 \cdot \mathbf{n}_0 + D_i\nabla_y\phi_1 \cdot \mathbf{n}_0)$$

$$+D_i\nabla_y\phi_0 \cdot \mathbf{n}_2 + D_i\nabla_x\phi_0 \cdot \mathbf{n}_1 + D_i\nabla_y\phi_1 \cdot \mathbf{n}_1 + D_i\nabla_x\phi_1 \cdot \mathbf{n}_0 + D_i\nabla_y\phi_2 \cdot \mathbf{n}_0 + p_f v_w(\psi_0 - \phi_0)\phi_0$$

$$+\frac{1}{2}(y,\Lambda\mathbf{n}_0) \cdot (\mathcal{D}^2(D_i\nabla_y\phi_0 \cdot \mathbf{n}_0)(y,\Lambda\mathbf{n}_0))\Big] + \epsilon^2(\cdots) = 0, \quad y \in \Gamma_0(x,t), \qquad (16)$$

where $\mathcal{D}^2$ is Hessian and the parameter Λ is related to the expansion of level set function G_ϵ in the following way [47]:

$$\Lambda = \frac{G_1}{|\nabla_y G_0|} - \frac{y \cdot \nabla_x G_0}{|\nabla_y G_0|}, \quad y \in \Gamma_0(x,t).$$

In a similar way, for the boundary condition

$$D_e \nabla \psi_\epsilon \cdot \mathbf{n}^\epsilon + \epsilon v_n \psi_\epsilon = 0, \tag{17}$$

by assigning ψ_ϵ and $\mathbf{n}^\epsilon$ in (17), we will have:

$$\frac{1}{\epsilon} D_e \nabla_y \psi_0 \cdot \mathbf{n}_0 + D_e \nabla_y \psi_0 \cdot \mathbf{n}_1 + D_e \nabla_x \psi_0 \cdot \mathbf{n}_0 + D_e \nabla_y \psi_1 \cdot \mathbf{n}_0 + y \cdot \nabla_x (D_e \nabla_y \psi_0 \cdot \mathbf{n}_0) + \lambda \mathbf{n}_0 \cdot \nabla_y (D_e \nabla_y \psi_0 \cdot \mathbf{n}_0)$$

$$+ \epsilon \Big[y \cdot \nabla_x (D_e \nabla_y \psi_0 \cdot \mathbf{n}_1 + D_e \nabla_x \psi_0 \cdot \mathbf{n}_0 + D_e \nabla_y \psi_1 \cdot \mathbf{n}_0) + \lambda \mathbf{n}_0 \cdot \nabla_y (D_e \nabla_y \psi_0 \cdot \mathbf{n}_1 + D_e \nabla_x \psi_0 \cdot \mathbf{n}_0 + D_e \nabla_y \psi_1 \cdot \mathbf{n}_0)$$

$$+ D_e \nabla_y \psi_0 \cdot \mathbf{n}_2 + D_e \nabla_x \psi_0 \cdot \mathbf{n}_1 + D_e \nabla_y \psi_1 \cdot \mathbf{n}_1 + D_e \nabla_x \psi_1 \cdot \mathbf{n}_0 + D_e \nabla_y \psi_2 \cdot \mathbf{n}_0 - p_f v_w (\psi_0 - \phi_0) \psi_0$$

$$+ \frac{1}{2} (y, \lambda \mathbf{n}_0) \cdot (\mathcal{D}^2 (D_i \nabla_y \psi_0 \cdot \mathbf{n}_0)(y, \lambda \mathbf{n}_0)) \Big] + \epsilon^2 (\cdots) = 0, \quad y \in \Gamma_0(x,t). \tag{18}$$

2. Lowest-order problems

We collect the ϵ^{-2}-term form (13) and ϵ^{-1}-term form (16) and obtain:

$$\nabla_y^2 \phi_0 = 0, \quad \nabla_y \phi_0 \cdot \mathbf{n}_0 = 0.$$

Because of periodicity in the y of ϕ_0, it follows that ϕ_0 is determined up to a constant and does not depend on y and that $\nabla_y \phi_0 = 0$. Similarly, ψ_0 is determined up to a constant and does not depend on y.

3. Reference cell problems

The multiscale approach of homogenization yields a boundary value problem that must be solved in order to determine the effective diffusivity. This boundary value problem, commonly referred to as the *cell problem*, is obtained by the next part of the asymptotic expansion of (13). We collect the ϵ^{-1} term from (13), the ϵ^0 term from (16), and, given $\nabla_y \phi_0 = 0$:

$$\begin{array}{ll} \nabla_y \cdot [D_i (\nabla_y \phi_1 + \nabla_x \phi_0)] = 0 & y \in Y_0^i(x,t) \\ D_i (\nabla_y \phi_1 + \nabla_x \phi_0) \cdot \mathbf{n}_0 = 0 & y \in \Gamma_0(x,t). \end{array} \tag{19}$$

We set the function $F = D_i (\nabla_x \phi_0 + \nabla_y \phi_1)$. We claim that $F = 0$.

We define the function

$$\alpha = \phi_1 + y \cdot \nabla_x \phi_0 + \bar{\alpha}(x,t).$$

From the system (19), we see that α is the solution of the following system:

$$\begin{array}{ll} \nabla_y \cdot (D_i \nabla_y \alpha) = 0 & y \in Y_0^i(x,t) \\ D_i \nabla_y \alpha \cdot \mathbf{n}_0 = 0 & y \in \Gamma_0(x,t). \end{array} \tag{20}$$

On the other hand, from the view of theory of partial differential equations, it is well known that the solutions of a linear homogeneous elliptic equation with zero Neumann boundary condition [like system (20)] are constants [48]. So the solutions of system (20) are independent of variable y. Thus the solution α of the system is the independent of variable y, and the derivative of α with respect to y is zero. This means that:

$$\nabla_y \alpha = \nabla_x \phi_0 + \nabla_y \phi_1 = 0$$

and

$$F = D_i (\nabla_x \phi_0 + \nabla_y \phi_1) = 0.$$

This prove the claim.

In the next step, we collect the ϵ^{-1} term from (14), the ϵ^0 term from (18), and, using that $\nabla_y \psi_0 = 0$:

$$\begin{array}{ll} \nabla_y \cdot [D_e (\nabla_y \psi_1)] = 0, & y \in Y_0^e(x,t) \\ D_e (\nabla_y \psi_1 + \nabla_x \psi_0) \cdot \mathbf{n}_0 = 0, & y \in \Gamma_0(x,t) \end{array}$$

So, the *cell problem* becomes:

$$\begin{array}{ll} \nabla_y \cdot (\nabla_y \omega_j) = 0, & y \in Y_0^e(x,t) \\ \nabla_y \omega_j \cdot \mathbf{n}_0 = -e_j \cdot \mathbf{n}_0, & y \in \Gamma_0(x,t) \\ \omega_j \text{ periodic in } y \end{array} \tag{21}$$

for $j = 1,2$, where $\psi_1 = \omega_1 \partial_{x_1} \psi_0 + \omega_2 \partial_{x_2} \psi_0$.

4. Homogenized problems

The third term in the expansion of intracellular and extracellular concentrations must be considered in order to obtain a first-term approximation. For extracellular concentration, we have:

$$\begin{array}{ll} \partial_t \psi_0 = \nabla_y \cdot (\nabla_y \psi_2 + \nabla_x \psi_1) + \nabla_x \cdot H & y \in Y_0^e(x,t) \\ y \cdot \nabla_x (H \cdot \mathbf{n}_0) + \lambda \mathbf{n}_0 \cdot \nabla_y (H \cdot \mathbf{n}_0) + H \cdot \mathbf{n}_1 & \\ + (\nabla_y \psi_2 + \nabla_x \psi_1) \cdot \mathbf{n}_0 + p_f v_w (\psi_0 - \phi_0) \psi_0 = 0 & y \in \Gamma_0(x,t) \end{array}, \tag{22}$$

where $H = D_e \nabla_x \psi_0 + D_e \nabla_y \psi_1$.

Next, we integrate the first (22) on $Y_0^e(x,t)$ with respect to y and apply the related boundary condition, and we will have:

$$\int_{Y_0^e(x,t)} \partial_t \psi_0 dy = \int_{Y_0^e(x,t)} \nabla_y \cdot (\nabla_y \psi_2 + \nabla_x \psi_1) + \nabla_x \cdot H dy$$

$$\left| Y_0^e(x,t) \right| \partial_t \psi_0 = \int_{\Gamma_0(x,t)} (\nabla_y \psi_2 + \nabla_x \psi_1) \cdot \mathbf{n}_0 dS(y) + \int_{Y_0(x,t)} \nabla_x \cdot H dy$$

$$= \int_{\Gamma_0(x,t)} [-y \cdot \nabla_x(H \cdot \mathbf{n}_0) - \lambda \mathbf{n}_0 \cdot \nabla_y(H \cdot \mathbf{n}_0) - H \cdot \mathbf{n}_1 - p_f v_w(\psi_0 - \phi_0)\psi_0] dS(y)$$

$$+ \int_{Y_0^e(x,t)} \nabla_x \cdot H dy \tag{23}$$

by applying the Reynold transport theorem in order to interchange integration and spatial derivation:

$$\nabla_x \cdot \int_{Y_0^e(x,t)} H dy = \int_{Y_0^e(x,t)} \nabla_x \cdot H dy - \int_{\Gamma_0(x,t)} \frac{\nabla_x G_0}{|\nabla_y G_0|} \cdot H dy. \tag{24}$$

Then, from (23) and (24), we will have:

$$\left|Y_0^e(x,t)\right| \partial_t \psi_0 = \nabla_x \cdot \int_{Y_0^e(x,t)} H dy - \int_{\Gamma_0(x,t)} p_f v_w(\psi_0 - \phi_0)\psi_0 dS(y) - I_1 - I_2,$$

where

$$I_1 = \int_{\Gamma_0(x,t)} y \cdot \nabla_x(H \cdot \mathbf{n}_0) - \frac{y \cdot \nabla_x G_0}{|\nabla_y G_0|} \mathbf{n}_0 \cdot \nabla_y(H \cdot \mathbf{n}_0) dS(y),$$

$$I_2 = \int_{\Gamma_0(x,t)} \frac{\tau_0 \cdot \nabla_y G_1}{|\nabla_y G_0|} \tau_0 \cdot H - \frac{G_1}{|\nabla_y G_0|} \cdot \nabla_y(H \cdot \mathbf{n}_0) dS(y).$$

and by using Lemma 3.1 and Lemma 3.2 in Ref. [47],

$$I_1 = I_2 = 0.$$

Next, we get the following partial differential equation for the ECS osmolarity concentration:

$$\left|Y_0^e(x,t)\right| \partial_t \psi_0 = \nabla_x \cdot (\bar{D}(x,t)\nabla_x \psi_0) - |\Gamma_0(x,t)| p_f v_w(\psi_0 - \phi_0)\psi_0,$$

where the tensor $\bar{D}(x,t) = (\bar{D}_{ij})_{i,j}$ is given by:

$$\bar{D}_{ij} = D \int_{Y_0^e(x,t)} (\delta_{ij} + \partial_{y_i} \omega_j) dy \tag{25}$$

and by the Reynolds transport theorem for time derivatives:

$$\partial_t \left(\left|Y_0^e(x,t)\right| \psi_0\right) = \nabla_x \cdot (\bar{D}(x,t)\nabla_x \psi_0) + \int_{\Gamma_0(x,t)} p_f v_w(\psi_0 - \phi_0)\psi_0 dS(y) - |\Gamma_0(x,t)| p_f v_w(\psi_0 - \phi_0)\psi_0. \tag{26}$$

Finally, from (26), we will have:

$$\partial_t \left(\left|Y_0^e(x,t)\right| \psi_0\right) = \nabla_x \cdot (\bar{D}(x,t)\nabla_x \psi_0). \tag{27}$$

For intracellular space, we have:

$$\begin{aligned} \partial_t \phi_0 &= \nabla_y \cdot (\nabla_y \phi_2 + \nabla_x \phi_1) + \nabla_x \cdot F & y \in Y_0^i(x,t) \\ y \cdot \nabla_x(F \cdot \mathbf{n}_0) &+ \lambda \eta_0 \cdot \nabla_y(F \cdot \mathbf{n}_0) + F \cdot \mathbf{n}_1 & \\ +(\nabla_y \phi_2 &+ \nabla_x \phi_1) \cdot \mathbf{n}_0 + p_f v_w(\psi_0 - \phi_0)\phi_0 = 0 & y \in \Gamma_0(x,t) \end{aligned}, \tag{28}$$

where we integrate the first (28) on $Y_0^i(x,t)$ with respect to y and apply the related boundary condition. In a similar way, since $F = 0$, we will have:

$$\partial_t \left(\left|Y_0^i(x,t)\right| \phi_0\right) = 0. \tag{29}$$

In the next section, through upscaling, we obtain a macroscopic description of the transport processes supplemented by the cell problem (21).

E. Upscaling

In the previous section, periodic homogenization was applied to the system of partial differential equations (7) and (8), describing diffusion transport of osmolarities within a porous medium in evolving domains. A level set formulation was used to handle the evolving microstructure. As a result of performing the averaging procedure using two-scale asymptotic expansion, we obtained a set of modified averaged diffusion equations for ECS and ICS osmolarities. These equations are supplemented by several families of microscopic cell problems.

From these, we derive averaged coefficient functions, which explicitly depend on space, time, microscopic geometry, osmolarity differences across the cell membrane, and membrane water permeability. These procedures lead to the following upscaling results for the dynamics of the ECS and ICS osmolarities:

$$\begin{aligned} \partial_t \left(\left|Y_0^e(x,t)\right| \psi_0\right) &= \nabla_x \cdot (\bar{D}(x,t)\nabla_x \psi_0), & x \in \Omega, t \in (0,T) \\ \partial_t \left(\left|Y_0^i(x,t)\right| \phi_0\right) &= 0, & x \in \Omega, t \in (0,T) \end{aligned}, \tag{30}$$

with sufficient initial and boundary conditions and diffusion tensor $\bar{D}(x,t)$ defined by:

$$\bar{D}(x,t) = D \int_{Y_0^e(x,t)} (\delta_{ij} + \partial_{y_i}\omega_j)dy, \tag{31}$$

where ω_j being the solutions of the cell problems (21). Furthermore, the level set function $G_0 = G_0(t,x,y)$ fulfills the following:

$$\partial_t G_0 + p_f v_w(\psi_0 - \phi_0)|\nabla_y G_0| = 0, \tag{32}$$

and $Y_0^e(x,t) = \{y : G_0(x,y,t) < 0\}$, $Y_0^i(x,t) = \{y : G_0(x,y,t) > 0\}$.

F. Tortuosity

The main result of the homogenization procedure coupled with the level set method in this study is the derivation of the tortuosity factor based on the relevant parameters. These parameters are time, space, the geometry of the reference cell, diffusivity in the ECS, osmolarity difference across the membrane, and cell membrane water permeability. We first set $D^*(x,t)$ as the following:

$$D^*(x,t) = \frac{\bar{D}(x,t)}{|Y_0^e(x,t)|} = \frac{D}{|Y_0^e(x,t)|} \int_{Y_0^e(x,t)} (\delta_{ij} + \partial_{y_i}\omega_j)dy.$$

Then this leads to the following expression for the definition of the tortuosity:

$$\frac{1}{\lambda^2(x,t)} = \frac{D^*(x,t)}{D} = \frac{1}{|Y_0^e(x,t)|} \int_{Y_0^e(x,t)} (\delta_{ij} + \partial_{y_i}\omega_j)dy. \tag{33}$$

To compute these relations, we should solve the coupling equations in (30), (31), (32), and the cell problem (21). In the following sections, we present the results of simulated numerical methods for solving these equations.

III. EXAMPLES

To illustrate the simulated numerical results of our model, we established a 2D geometry as a selected tissue of the brain and calculated the tortuosity and volume fraction in a few physiologically relevant example conditions. The solution of the coupled equations in (30), (31), (32), and the cell problem (21) is technically interesting. The main difficulty of

the numerical algorithm for solving these equations is the fact that the microstructure of the porous medium is evolving due to the osmotic process. Additional difficulties are nonlinearity of these equations and coupling them.

We applied the numerical algorithm that was proposed in Ref. [49]. We used the implicit Euler method in order to obtain a sequence of discrete-time coupled systems. Spatial discretization was performed by using finite element method (FEM) for our simulations and numerical schemes.

In this work, we model the cells as square tiles with initial length 0.45 μm. The tissue selected for simulation is taken to be $\Omega = [0,J] \times [0,J]$, with the length $J = 100$ μm. Also, we denote the initial osmolarity difference across the membrane as $\sigma = \phi(x,0) - \psi(x,0)$. Values and units of the parameter that are used in the simulation are indicated in Table I.

Today it is well established that the ECS constitutes about 15–20% of the normal adult brain tissue volume and that this figure falls to 5% during ischemia [17]. We considered the initial volume fraction as 19%, which means that $\alpha(x,0) = 0.19$.

Water transport across the ICS-ECS interface is driven by the difference in ICS and ECS osmolarities. Cell membrane water permeability is mediated by AQP4 water channels. Water transport between the ICS and ECS compartments result in displacement of the ICS-ECS interface, with water influx causing ECS contraction and cell expansion.

For our computational purposes, we discuss some simplification in Eq. (32) of the effective model equations presented in the upscaling section above. We consider a geometrical setting in which the cells are of square shape at initial time (see Fig. 3). The solution of level set equation (32) for all $x \in \Omega$ and $t > 0$ is shown by the dashed-line square in Fig. 3, [33,34]. For simplification of our computations and for comparison of our results to previous data, we approximate the dashed-line square with the solid-line square (Fig. 3). By this assumption, (32) can be reduced to

$$\frac{\partial h}{\partial t}(x,t) = -p_f v_w[\psi_0(x,t) - \phi_0(x,t)], \tag{34}$$

where h is the length of the square cell shape.

In what follows, a fully discrete numerical scheme is presented, which is capable of approximating the effective quantities of interest. This incorporates the solving of the system (30), (31), (34), as well as the cell problem (21). We apply

TABLE I. Model parameters.

Parameter	Value	Description	Reference
$\phi(x,t)$	–	Osmolarity of the ICS (mol/m^3)	–
$\psi(x,t)$	–	Osmolarity of the ECS (mol/m^3)	–
D_e	10^{-4}	Diffusion coefficient of osmolyte in ECS (cm^2/s)	–
D_i	10^{-4}	Diffusion coefficient of osmolyte in ICS (cm^2/s)	–
p_f	0.001, 0.002, 0.004, 0.008	Membrane water permeability (cm/s)	[50,51]
v_w	18	Partial molar volume of water (cm^3/mol)	[50]
λ	–	Tortuosity	–
σ	–	$\psi(x,0) - \phi(x,0)$	–
t	–	Time (s)	–
x	–	Space	–
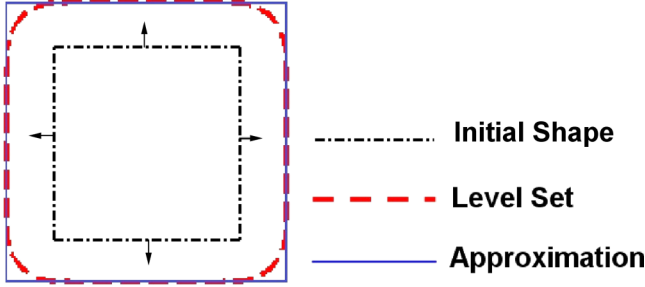
FIG. 3. The initial shape of the cell is represented by the dash-dotted line. Using this initial shape, the solution of our level set equation (32) is represented by the dashed line, which is approximated by the square shape that is represented by the solid line.

Rothe's method to the system using the implicit Euler method in order to obtain a sequence of discrete-time, yet still coupled, systems. The couplings between the microscopic scale and the macroscopic scale and also the couplings between the length of square are resolved by an iterative splitting scheme.

Spatial discretization is performed on unstructured triangular grids by finite elements for both the macroscopic problems and the cell problems.

Time discretization: Let $0 =: t_0 < t_1 < \cdots < t_N$ be a not-necessarily equidistant decomposition of the time interval $I =]0,T[$ and let $t_n - t_{n-1} =: \eta_n$ denote the time step size. Furthermore, for any time-dependent quantity $u(x,t)$, we use the notation $u^n = u^n(x) = u(t_n,x)$. Application of the implicit Euler method yields a sequence of N stationary yet coupled systems. More precisely, for $n = 1, \ldots, N$ we have to find $(\psi_0^n, \phi_0^n, h^n)$ in terms of $\psi_0^{n-1}(x)$, $\phi_0^{n-1}(x)$, $h^{n-1}(x)$, and $\bar{D}^{n-1}(x)$ with coefficients $\bar{D}^n(x)$ which in turn depend in particular on $h^n(x)$.

Spatial discretization: Let $\mathcal{T}_K = \{T\}$ be a regular decomposition of the macroscopic domain Ω into closed triangles T of characteristic size H such that $\bar{\Omega} = \bigcup T$. We call the associated mesh of $\mathcal{T}_K$ the coarse-scale grid, represented by the same symbol. Each triangle $T \in \mathcal{T}_K$ is associated with a unit cell Y_0^T containing an evolving ECS space $Y_{0,e}^T = Y_{0,e}^T(t)$ that is clearly time dependent due to the evolving interface and that is denoted by $Y_{0,e}^{T,n}$ for the time level t_n. Analogously, let $T_k = T_k^{n,T}$ denote the family of fine-scale grids covering the domains $Y_{0,e}^{T,n}$, $T \in \mathcal{T}_K$. We denote by $\mathbb{P}_m(T)$ the space of polynomials of degree at most m on T and $\mathbb{P}_m(\mathcal{T}_K) = \{\omega_K : \Omega \longrightarrow \mathbb{R} | \forall T \in \mathcal{T}_K, \omega_k | T \in \mathbb{P}_m(T)\}$. In order to approximate the vector and scalar unknowns of (30) and cell problem (21), we use the spaces $\mathbb{P}_1(\mathcal{T}_K)$ and $\mathbb{P}_1(\mathcal{T}_k)$.

We skip the variational formulation of the discrete-time macroscopic system (30) and of the cell problems (21), which are beyond the scope of this paper. Instead, we refer to Ref. [52] and indicate only the major points of the discretization.

We state our solution strategy by means of the following algorithm.

Algorithm:

Initialization
   Let $n = 0$. Generate a coarse-scale grid $\mathcal{T}_K = \mathcal{T}_K(\Omega_0)$, initialize $\phi_{0,K}^n$, $\psi_{0,K}^n$, $h_{0,K}^n$, and choose a fixed time step size $\tau_n = \tau$.

Time Step
   (1) *Set $n := n + 1$. If $t_n = t_N$, then terminate.*
   (2) *For each triangle $T \in \mathcal{T}_K$, generate fine-scale grids $\mathcal{T}_k(Y_{0,e}^{T,n})$ using the coarse scale $h_{K,0}^{n-1}$ and an appropriate mesh sizes.*
   (3) *For each triangle $T \in \mathcal{T}_K$, solve the cell problem (21) on $Y_{0,e}^{T,n}$ in order to compute the coarse-scale coefficients $\bar{D}_K^n$.*
   (4) *Solve (30), $\phi_{0,K}^n$, and $\psi_{0,K}^n$ using $\bar{D}_K^n$.*
   (5) *Solve (34) for $h_{0,K}^n$ using $\phi_{0,K}^n$ and $\psi_{0,K}^n$.*
   (6) *Proceed with (1).*

Postprocessing
   For all time levels t_n, compute the coarse-scale porosity $Y_{0,e,K}^n$ using $h_{0,K}^n$ and the coarse-scale $\phi_{0,K}^n$ and $\psi_{0,K}^n$.

Remark: We use fixed time step size $\tau_n = 0.01$. At the first and last time levels, we use a coarse-scale grid $\mathcal{T}_K$ consisting of 5645 triangles. For fixed $t = t_n$ these are covered by fine-scale grids $T_k, T \in \mathcal{T}_K$ consisting of 1000 to 7000 triangles.

A. Tortuosity as a function of ECS volume fraction

The earliest model of this class is what was described by Maxwell. His result ($\lambda = \sqrt{2 - \alpha}$) was originally derived for a dilute suspension of spheres where α is close to unity. In fact, spheres neither fill the 2D space nor pack closely, and the limiting values close to zero of α are unattainable. But in our model, squares can fill the 2D space and pack closely. It follows that the limiting values $\alpha \to 0$ are applicable to these packed geometry on small values of α.

Our results (Fig. 4) show that for packed squares λ increases slowly to a finite value of $\sqrt{2} = 1.414$ for the limiting values $\alpha \to 0$, the well-known limit for λ in 2D [13,14], even though Maxwell's assumptions are severely violated under these circumstances. This is consistent with the conclusion on λ for limiting values of α presented in Refs. [13,14]. This is probably the reason why equation $\lambda = \sqrt{2 - \alpha}$ works fairly well for a wide range of well-connected ECS volume fractions (see Fig. 4). So, the extension of the Maxwell formula to packed square cells with uniform spacing is valid for the small values of α.
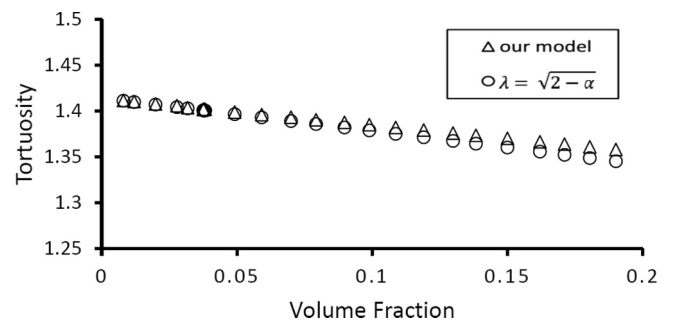
FIG. 4. Tortuosity plotted as a function of volume fraction. A comparison is made between our model prediction and the formula $\lambda = \sqrt{2 - \alpha}$.
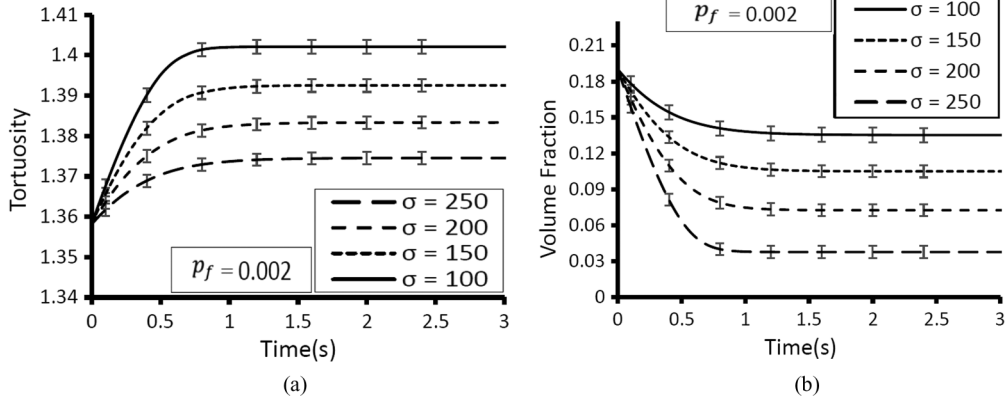
FIG. 5. (a) Tortuosity (λ) plotted as a function of time for multiple values of initial osmolarity difference across the cellular membrane (σ). (b) Volume fraction α plotted as a function of time for multiple values of initial osmolarity difference across the cellular membrane (σ). Values and units of these parameters are given in Table I.

B. Time evolution of tortuosity and volume fraction against osmolarity gradient

First we studied the temporal behavior of the tortuosity factor (Fig. 5) for multiple values of initial osmolarity difference with a fixed membrane permeability. The time course of tortuosity is plotted according to initial osmolarity differences of $\sigma = 100, 150, 200,$ and 250 mol/m^3 and cell membrane water permeability of $p_f = 0.002$ cm/s. As shown in the figure, tortuosity increases and volume fraction decreases when the initial osmolarity difference is higher. The low initial osmolarity difference (i.e., $\sigma = 100$ mol/m^3) leads to a significant decrease in α and a small increase in λ. However, a high initial osmolarity difference (i.e., $\sigma = 250$ mol/m^3) leads to a larger decrease in α and a larger increase in λ.

Brain cells swell when exposed to hypotonic media or during ischemia, with reciprocal changes in the ECS [53,54]. Information about global ECS changes during global cerebral ischemia has been very limited. One of the applications of our model is in explaining the changes of molecular diffusion during global cerebral ischemia. As shown in Fig. 5(b), for $p_f = 0.002$ cm/s and $\sigma = 250$ mol/m^3, volume fraction decreases from 19% to 4%, which is consistent with the decreased volume of ECS volume during ischemia.

C. Time evolution of tortuosity and volume fraction against membrane permeability

Next, we studied the temporal behavior of tortuosity and volume fraction (Fig. 6) for several values of cell membrane water permeability, $p_f = 0.001, 0.002, 0.004,$ and 0.008 cm/s, with a fixed osmolarity difference of $\sigma = 150$ mol/m^3. As shown, by reducing water permeability (e.g., with AQP4 inhibition or deletion), the rate of decrease in volume fraction and the rate of increase in tortuosity are both reduced.

In physiological context, such delayed increase of the volume fraction and delayed increase of tortuosity are observed following the AQP4 deletion [55].

The above results demonstrate an equilibrium phenomenon in our model, which is a crucial behavior of many physical systems. These results show that increasing the initial osmolarity difference has very little effect on osmolarity equilibrium time. In contrast, an increase in membrane water permeability has a strong effect on the equilibrium time because it allows faster water flow.

D. Case of nonuniform osmolarity distribution

In the previous case studies, we assumed that the initial osmolarities in the ECS and ICS are distributed uniformly,
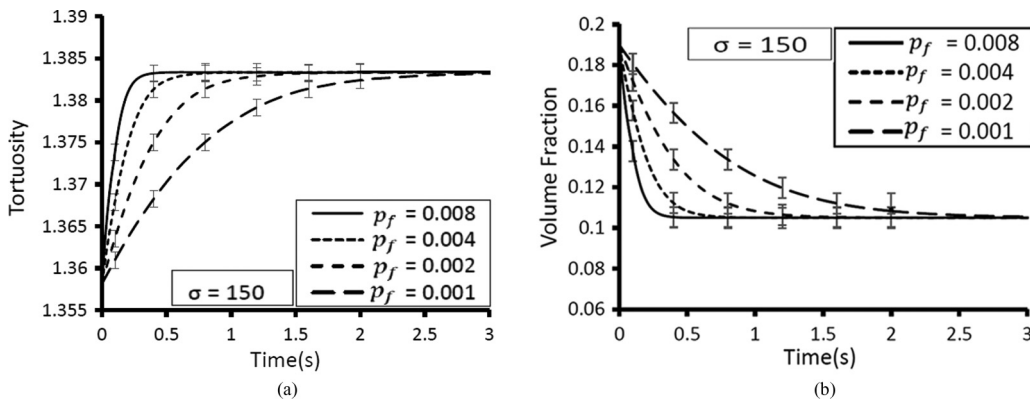
FIG. 6. (a) Tortuosity (λ) plotted as a function of time for multiple values of water permeability of the membrane (p_f). (b) Volume fraction (α) plotted as a function of time for multiple values of membrane water permeability (p_f). Values and units of these parameters are given in Table I.

i.e., σ is constant throughout the selected tissue. However, under some physiological conditions, such as focal ischemia, the osmolarity difference across the membranes is confined to a specific region of the brain [56]. Our model is able, to some extent, to explain the time course of tortuosity and volume fraction changes in such a localized situation. In this case, we assume that $p_f = 0.004$ cm/s and that the initial osmolarities are distributed nonuniformly in the ECS and uniformly in the ICS, with the following equation:

$$\psi(x,0) = \begin{cases} 150 & x_1^2 + x_2^2 \leqslant 10, \\ 300 & \text{else} \end{cases}, \qquad \phi(x,0) = 300, \tag{35}$$

where, $x = (x_1, x_2)$ is spatial coordinate. Equation (35) indicates that initial ECS osmolarity in the small circular region in the tissue is 150 mol/m^3 and in other regions of the tissue is 300 mol/m^3, and initial ICS osmolarity in all regions of the tissue is 300 mol/m^3 [see Fig. 7(a)]. More precisely, the only initial osmolarity difference exists at the boundary of the small circular region, and there is no initial osmolarity difference in the rest of the selected tissue. As shown in Fig. 7(b), changes of tortuosity in region A, where there is a difference in osmolarity, is higher than the other locations, i.e., B, C, and D. As illustrated, a decrease of volume fraction and increase of local tortuosity occurs near the region of osmolarity difference. This shows that tortuosity temporarily increases only in the ischemic region of the brain. It also shows that tortuosity does not depend on time alone but on spatial coordinates as well.

According to our results, the change in tortuosity caused by global ischemia is delayed compared to focal ischemia. Moreover, although changes in tortuosity occur globally, they most profoundly affect the ischemic region and adjacent areas. This finding may be important for developing neuroprotective strategies based on regional brain ischemia in experimental models.

E. Microscale and macroscale comparison

Last but not least, we compare numerical solutions of the original equations at the microscopic scale with numerical solutions of the homogenized model in order to see how well the homogenization technique approximates the real solutions to the original microscopic problem. For this purpose, we compare the solutions of the homogenized equations (30), (31), and (32) with the solutions of Eqs. (7) and (8) in the original microscopic model. The numerical simulation is performed in two cases, where the initial osmolarities are either uniformly or nonuniformly distributed in the selected domains.

In the case of uniformly distributed initial osmolarity, we use the constant water permeability $p_f = 0.008$ cm/s, and consider the initial conditions $\phi(x,0) = 300$ mol/m^3 in the ICS domain and $\psi(x,0) = 200$ mol/m^3 in the ECS domain. In Fig. 8(a) the time course of the ICS concentration ϕ_0 in the homogenized model and the ICS concentration ϕ_ϵ in the microscopic model are compared in a point inside the ICS. In Fig. 8(b) the time course of the ECS concentration ψ_0 in the homogenized model and the ECS concentration ψ_ϵ in the microscopic model are compared in a point inside the ECS.

In the case of nonuniformly distributed initial osmolarity, we use the constant water permeability $p_f = 0.004$ cm/s and consider the initial conditions in the relation (35). In Fig. 9(a) the time course of the ICS concentration ϕ_0 in the homogenized model and the ICS concentration ϕ_ϵ in the microscopic model are compared in a point inside the ICS. In Fig. 9(b) the time course of the ECS concentration ψ_0 in the homogenized model and the ECS concentration ψ_ϵ in the microscopic model are compared in a point inside the ECS.

The numerical simulation results show that the solution of the homogenized model well agrees with the solution of the microscopic model.

IV. DISCUSSION

Molecular diffusion in the brain ECS is an important topic in neuroscience research and drug delivery. Molecular diffusion depends, among other factors, on the ECS geometry, which is a complex and dynamic structure. In many physiological as well as pathological states, the ECS geometry is not stable and is affected by cell (especially glial) volume change [19]. This is

(a)   (b)
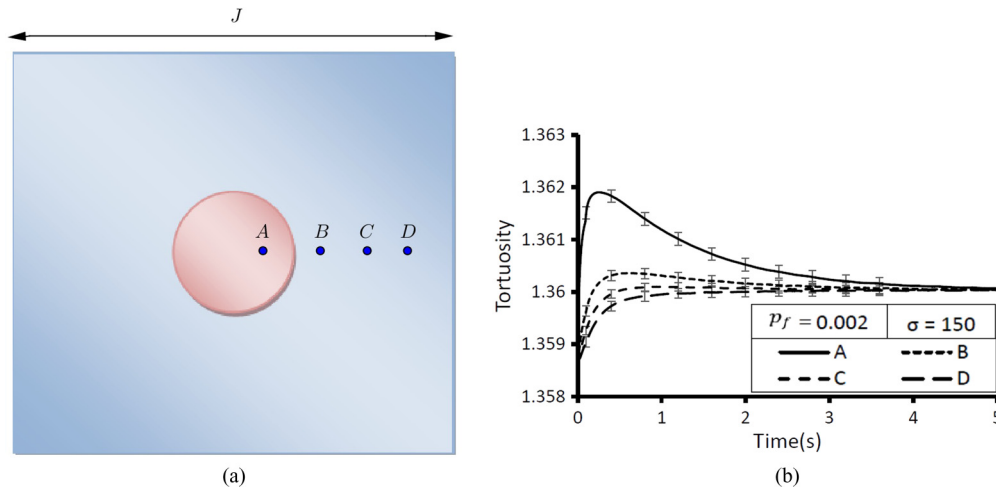
FIG. 7. (a) Nonuniform initial distribution of osmolarities in the selected tissue. Initial ECS osmolarity in the small circular region in the tissue is 150 mol/m^3 and in other regions of the tissue is 300 mol/m^3. Initial ICS osmolarity is 300 mol/m^3 throughout. (b) Tortuosity plotted as a function of time for the points A, B, C, and D. Values and units of these parameters are given in Table I.
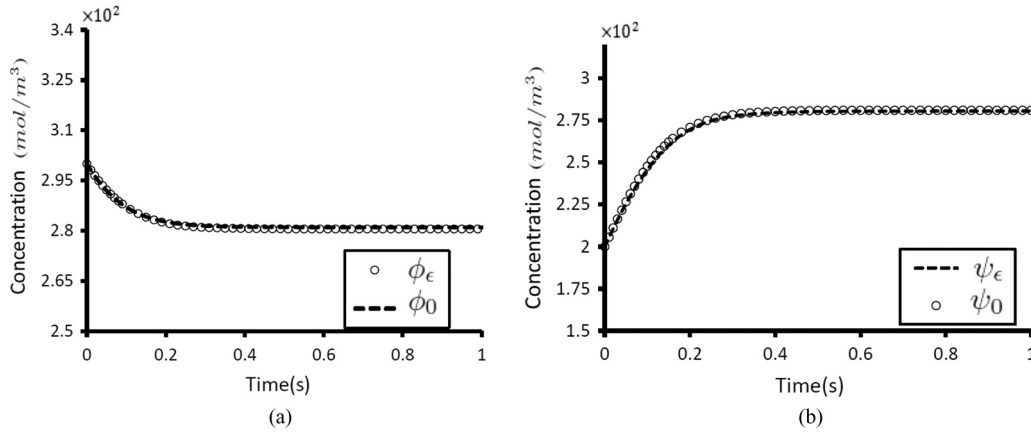
FIG. 8. Comparison of concentration profiles as a function of time between the microscopic model and the homogenized model in the case of nonuniformly distributed initial osmolarity. (a) The circles are the concentration of ϕ_ϵ in the microscopic model and the dashed line is the the concentration of ϕ_0 in the homogenized model. (b) The dashed line is the concentration of ψ_ϵ in the microscopic model and the circles are the concentration of ψ_0 in the homogenized model.

due to the movement of water between intra- and extracellular compartments in response to osmotic challenges. Water movement across the cellular membranes in the brain takes place via AQP4 water channels. Modulation of AQP4 expression has been shown to be effective in the treatment of water imbalance in various pathological states of the brain [57,58].

Changes in the diffusion parameters due to water transport influence both synaptic and extrasynaptic transmission. These changes may enhance or suppress neuronal activity or the accumulation of neuroactive substances (e.g., glutamate) due to changes in ECS volume. Information about these changes may be valuable for diagnostic or therapeutic purposes [1,59].

Because of the complex interplay between osmosis, membrane permeability, and ECS geometry, studying diffusion under different osmotic conditions requires quantitative models. To model the role of spatiotemporally nonlinear ECS dynamics in the brain, it is essential to develop computationally efficient descriptions for molecular diffusion in the tissue. The main objective of this paper has been to provide, for the first time, a comprehensive mathematical and computational framework for such dynamic processes. We studied diffusion, osmosis,

ECS geometry, and their interplay, all physical phenomena. We showed that the interplay between diffusion and osmosis can give the brain ECS a new property, which is reflected in its dynamic geometry and tortuosity.

We demonstrated how such a multiscale framework can be constructed using a homogenization theory coupled with the level set method. By using a level set formulation, we performed periodic homogenization of a coupled model describing ECS and ICS osmolarity dynamics within a porous medium as a selected brain tissue. In this process, we used the level set method to model the movement of cellular membranes with a velocity that is proportional to osmolarity difference across the cell membrane. Through this, we related cell membrane water permeability to diffusion parameters of the ECS.

The main outcome of our approach is establishment of a clear relation between the effective diffusion coefficient from a spatially averaged model and the original microscopic model. We demonstrated how homogenized equations can be used as appropriate and efficient tools to interpret the parameters of the original problem, as well as the time course of changes in these
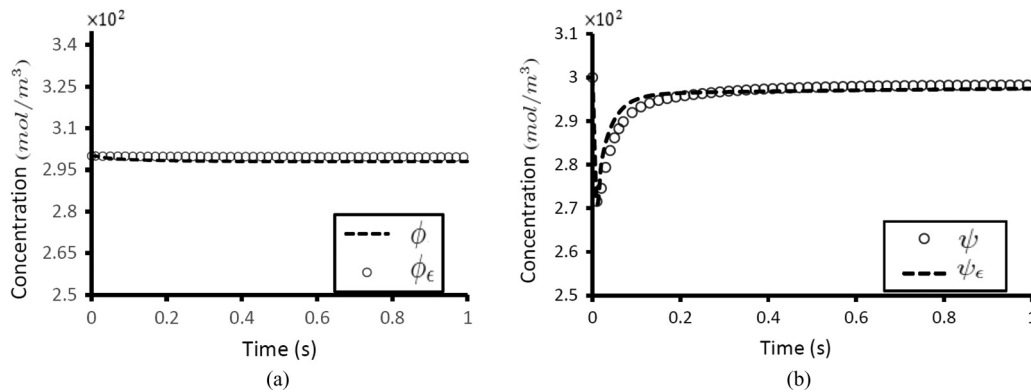
FIG. 9. Comparison of concentration profiles as a function of time between the microscopic model and the homogenized model in the case of nonuniformly distributed initial osmolarity. (a) The circles are the concentration of ϕ_ϵ in the microscopic model and the dashed line is the concentration of ϕ_0 in the homogenized model. (b) The circles are the concentration of ψ_ϵ in the microscopic model and the dashed line is the concentration of ψ_0 in the homogenized model.

parameters. Homogenization is required not only to derive the averaged equation but also to enable coupling of osmosis and diffusion parameters with dynamic geometrical variations of the ECS, independent of the uniformity or nonuniformity of the initial concentration distribution.

A key prerequisite of the homogenization technique is a wide separation of geometric length scales, which is clearly satisfied for the ECS. In fact, the characteristic size of the ECS is much smaller than the characteristic length scales of the representative brain tissue. The homogenization theory and level set method have been widely used to study various other phenomena in physics, engineering, and biology, and useful descriptions of their features have been provided in the literature [42,43,60,61].

Various computational approaches have been used for the investigation of diffusion parameters in the brain ECS [13–15,62]. However, the approaches have not illustrated the effect of cell membrane water permeability on diffusion parameters. Also, the time course of this dynamic effect has been unknown. Coupling the time-dependent equations of geometry, concentration gradient, water flux, osmolarity, and molecular diffusion renders the system strictly nonlinear. The interplay between these parameters is nonlinear as well, as demonstrated in our numerical simulations. In each simulation, although the final solute concentrations would be easily predictable by the initial equations, the goal of our model and numerical simulations is not to reach to the final equilibrium values but to demonstrate and analyze the nonlinear temporal dynamics of getting to that state from various initial states of the system.

Our model predicts, for the first time, the sensitivity of tortuosity to volume fraction, cell size, time, cell membrane water permeability, and osmolarity differences across the cell membrane. Our model can be used to understand the consequent effects of acute brain cell swelling, which results in ECS contraction and is seen in many pathologic conditions such as cerebral edema. Also, it can be concluded that the diffusion rate of neuroactive substances is modulated not only by the size of the pores between the cells but also by the dynamic changes of the ECS. This new understanding may reveal new targets for potential therapeutic interventions during brain pathologies associated with cell swelling, such as ischemia.

Our model and simulations were constructed and performed in two dimensions. The next natural step would be to extend the model to a realistic 3D setting. To this end, either the methods applied in this study need to be further developed or different approaches have to be used. For extending the model to three dimensions, one should modify the parameters on homogenization using the level set equation.

One major question addressed in this paper was whether reduced cell membrane water permeability (for example, in AQP4 deficiency) could, by itself, account for the altered ECS tortuosity dynamics, and, if so, how much the cell water permeability is reduced in AQP4 deficiency. The model makes predictions about the magnitude of reduction in cell water permeability needed to account for the observed experimental data [31,55,63]. AQP4, the predominant water channel in the brain, is mainly expressed in the glia and is not homogeneously distributed in the cell membrane. This inhomogeneous distribution of AQP4 may be a key point for better understanding the biological function of this water channel. For the purpose of the

current study, we assumed that water channels are distributed uniformly in the cell membranes. This simplification allows for studying the influence of high water permeable membranes on the volume fraction and tortuosity factor.

The studied effect (change in tortuosity caused by water transport) is small here, mainly because we are looking at the global tissue level scale. This is supported by previously published experimental observation in rodent brains [31,55,63]. However, such an effect may be more pronounced if we get down to molecular level and consider variations in tortuosity and diffusion coefficient of molecules from the ion channels or receptors perspective (microdomain). This encourages future models with water channels distributed nonuniformly in the membrane.

In the real world, the assumption that the cell membrane is only permeable to water holds true only in short time scales since the effect of membrane ion transport including the active transport through Na-K-ATPase also comes into play and may cancel out the observed effects of water transport on tortuosity. There is a phenomenological model that has studied such long-term coupling between water transport through AQP4 in the brain and other passive and active transports [64].

The tortuosity changes in our model and the resulting changes in molecular diffusion in the ECS can play a role in the function of passive ion transporters with high conductance such as Kir 4.1- inward rectifying potassium channel expressed in glial cells with conductance $G_{\text{Kir4.1}} = 27\,pS$ [65]. This assumption leads to the effects of water transport on tortuosity described in Fig. 5 and Fig. 6 at the maximum possible at the global scale, as water transport and volume change take place at their maximum rate. This is because there will be no reduction in the osmotic challenge caused by the solute transport.

In our model, anomalous diffusion processes in various distinct physical mechanisms are considered in terms of effective time- and space-dependent diffusivities. Combinations of space- and time-dependent diffusivities in theoretical considerations were investigated in Ref. [66]. Anisotropies in water diffusion have been observed in biological tissues with directional fibrous structure, for example, in the white matter of the human brain [67]. Measurement of such diffusional anisotropy (i.e., fractional anisotropy, axial diffusivity, and radial diffusivity) through diffusion-weighted magnetic resonance imaging (MRI) and diffusion tensor imaging serves as the basis of numerous studies of structural and functional connectivity in the human cerebral cortex, including the human connectome project [68].

Detection of early microstructural changes of neurodegeneration from bulk measurements of diffusivity on MRI is of great clinical interest for early detection of Alzheimer's disease and other dementias [69]. In the literature, restricted or hindered diffusion in various porous media has been considered in terms of effective time-dependent diffusivities. Controlled variation of the diffusion time, and corresponding modulation of the degree of restricted diffusion, can provide enhanced specificity and quantification of such properties as pore size, shape, connectivity, and permeability. The initial reduction of measured diffusion below its bulk value at short diffusion time is given by the ratio of the diffusion length to the confining length scale (or, more generally, to the inverse surface-to-volume ratio). On the other hand, very long diffusion times

are more widely feasible, especially in the clinic, and can maximize restricted diffusion contrast. Recently, the concept of time-dependent diffusivities in long times has been applied to interpret signals in nuclear magnetic resonance experiments and diffusion magnetic resonance imaging (dMRI) [67,70]. In Ref. [67], the following equation has been proposed for identifying the time-dependent instantaneous diffusion coefficient [$D_{inst}(t)$], which is accessible with techniques measuring the mean-square molecular displacement for the universality classes of disordered media with permeable barriers:

$$D_{inst}(t) = D_\infty + \text{const.} t^{-\theta},$$

where the dynamical exponent θ was related to the structural exponent p of the disorder as $\theta = (p + d)/2$ (d is the spatial dimension) and approaches the finite bulk diffusion constant D_∞. The structural exponent can be defined from the asymptotic behavior of the Fourier transform of the two-point structure correlation function: $\Gamma(k) \sim k^p$ as $k \to 0$. Structural universality classes of the medium can be distinguished by the exponent p: the ordered periodic arrangement ($p = \infty$), short-range disorder with a finite correlation length ($p = 0$), or strong disorder ($p < 0$) that can be achieved. The relation between the structural exponent and the dynamical exponent allows one to determine from dMRI the most appropriate kind of model for mesoscopic structural disorder. In particular, authors in Ref. [67] identified the relevant microscopic structure affecting water diffusion measured with dMRI in muscles and in brain and elucidated the corresponding microscopic changes providing clinically relevant dMRI contrast in ischemic stroke.

The above studies [67,70] seek to estimate tissue microstructural geometry from bulk measurements of diffusivity at equilibrium, i.e., when $t \to \infty$. Our model, in contrast, demonstrates the dynamics of reaching to that equilibrium state when the osmotic equilibrium is disturbed.

Finally, it is worth noting that ECS is characterized by both its geometry and content (extracellular matrix; ECM) [59]. While the ECS geometry is a global factor influencing diffusion of all molecules, the ECM affects only diffusion of molecules that interact with it, either electrostatically or sterically. The ECM impact on diffusion depends on its concentration and distribution in the ECS and thus would change during dynamic ECS changes. Studying the ECM effects is outside the scope of this paper. For even more detailed studies, the transport of ions such as potassium, sodium, and chloride in the ECS and their corresponding membrane transport mechanisms are also needed to fully characterize the system.

V. CONCLUSION

We provided a unified multiscale mathematical and computational framework for studying diffusion in biological tissues in general and in the brain in particular. The model uniquely binds, dynamically in time and space, the ECS volume fraction and tortuosity with cell membrane water permeability and osmotic gradient across the membrane. We presented multiple numerical simulations, using this framework, that either demonstrate or predict dynamic ECS changes under various common physiologic and pathologic conditions, including uniform and nonuniform osmolarity distributions, in both microscale and macroscale. Our model can be used as a

first step towards studying more complicated and biologically relevant systems.

APPENDIX

Here we describe the details of the derivation of the boundary condition presented in Sec. II C, the mathematical formulation of our model. First, we assume that v is the velocity of the membrane and $v_n = v \cdot \mathbf{n}$ is the normal velocity of the membrane so $\mathbf{n}$ is the unit normal which pointing into the ICS. Let $t > 0$ and $x \in \gamma(t)$ be given in which $\gamma(t)$ is a boundary on a single cell. Consider a cylinder of radius $\delta > 0$, with the axis intersecting $\gamma(t)$, normal to $\gamma(t)$, and x in the center of cylinder (Fig. 10). Bound this cylinder by a fixed disk at distance δ from x and the portion of $\gamma(t)$ inside the membrane. This is a cylinder-like portion of space, with one face evolving through time which is denoted by $\Upsilon_{t,\delta}$. Denote this small portion of space at time t by $\Sigma_{t,\delta}$. After a small time Δt, the face containing x has moved a little due to boundary movement, while the other face has not moved. The flux into the cylinder is given by:

$$\int_{\partial \Sigma_{t,\delta}} D_e \nabla\phi \cdot \mathbf{n}\, dS$$

and since the membrane (Υ_t) is impermeable to solutes, then the net flux into the Σ_t is

$$\int_{\partial \Sigma_{t,\delta} - \Upsilon_{t,\delta}} D_e \nabla\phi \cdot \mathbf{n}\, dS. \tag{A1}$$

On the other hand, the total amount of the property $\psi(t)$ within the control volume Σ_t is given by:

$$M(t) = \int_{\Sigma_{t,\delta}} \phi\, dV.$$
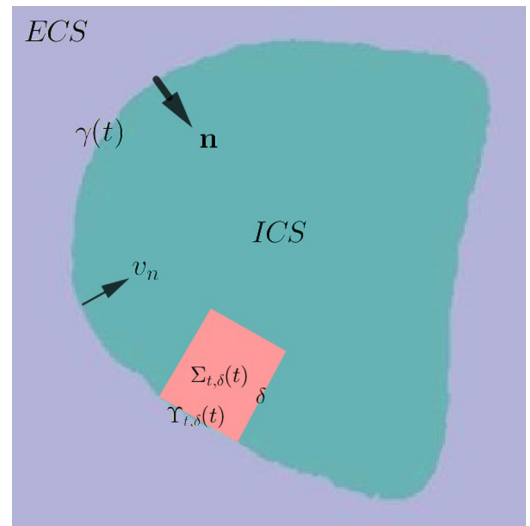
FIG. 10. Impression of a typical cell and the selected square region in it.

For moving interface, the Reynolds transport theorem can be stated as:

$$\frac{dM(t)}{dt} = \int_{\Sigma_{t,\delta}} \frac{\partial \phi}{\partial t} dV + \int_{\partial \Sigma_{t,\delta}} v_n \phi \, dS \qquad (A2)$$

and by using (2) and (A2) the Divergence theorem yields:

$$\frac{dM(t)}{dt} = \int_{\partial \Sigma_{t,\delta}} D_e \boldsymbol{\nabla} \phi \cdot \mathbf{n} + v_n \phi \, dS.$$

Since except Υ_t, the other sides of $\Sigma_{t,\delta}$ are not moving, we have:

$$\frac{dM(t)}{dt} = \int_{\partial \Sigma_{t,\delta}} D_e \boldsymbol{\nabla} \phi \cdot \mathbf{n} + \int_{\Upsilon_{t,\delta}} v_n \phi \, dS \qquad (A3)$$

by using (A1) and (A3) and conservation law of mass:

$$\int_{\Upsilon_{t,\delta}} D_e \boldsymbol{\nabla} \phi \cdot \mathbf{n} + v_n \phi \, dS = 0$$

and by $\delta \longrightarrow 0$, we have the boundary condition:

$$D_e \boldsymbol{\nabla} \phi(x,t) \cdot \mathbf{n} + v_n(x,t) \phi(x,t) = 0. \qquad (A4)$$

[1] L. Vargová and E. Syková, Philos. Trans. R. Soc. Lond. B **369**, 20130608 (2014).

[2] L. F. Agnati, M. Zoli, I. Stromberg, and K. Fuxe, Neuroscience **69**, 711 (1995).

[3] P. Bach-y-Rita, Cephalalgia **14**, 396 (1994).

[4] E. Sykova, Neuroscientist **3**, 28 (1997).

[5] L. L. Latour, K. Svoboda, and P. P. Mitra, Proc. Natl. Acad. Sci. USA **91**, 1229 (1994).

[6] A. Szafer, J. Zhong, and J. C. Gore, Magn. Reson. Med. **33**, 697 (1995).

[7] C. E. Krewson, M. L. Klarman, and W. M. Saltzman, Brain Res. **680**, 196 (1995).

[8] D. J. Wolak and R. G. Thorne, Mol. Pharmaceut. **10**, 1492 (2013).

[9] C. Nicholson and J. M. Phillips, J. Physiol. **321**, 225 (1981).

[10] C. Nicholson, Rep. Prog. Phys. **64**, 815 (2001).

[11] C. Nicholson and E. Syková, Trends Neurosci. **21**, 207 (1998).

[12] P. Kamali-Zare and C. Nicholson, Basic Clin. Neurosci. **4**, 282 (2013).

[13] K. C. Chen and C. Nicholson, Proc. Natl. Acad. Sci. USA **97**, 8306 (2000).

[14] J. Hrabe, S. Hrabetova, and K. Segeth, Biophys. J. **87**, 1606 (2004).

[15] R. K. Nandigam and D. M. Kroll, Biophys. J. **92**, 3368 (2007).

[16] S. Hrabetova and J. Hrabe, *Encyclopedia of Computational Neuroscience* (Springer, New York, 2015), pp. 434–437.

[17] A. Van der Toorn, E. Syková, R. M. Dijkhuizen, I. Voříšek, L. Vargová, E. Škobisová, M. van Lookeren Campagne, T. Reese and K. Nicolay, Magn. Reson. Med. **36**, 52 (1996).

[18] A. Homola, N. Zoremba, K. Slais, R. Kuhlen, and E. Sykova, Neurosci. Lett. **404**, 137 (2006).

[19] N. Zoremba, A. Homola, K. Slais, I. Vorisek, R. Rossaint, A. Lehmenkuhler, and E. Sykova, J. Cereb. Blood Flow Metab. **28**, 1665 (2008).

[20] E. A. Nagelhus, T. M. Mathiisen, and O. P. Ottersen, Neuroscience **129**, 905 (2004).

[21] M. Amiry-Moghaddam, D. S. Frydenlund, and O. P. Ottersen, Neuroscience **129**, 997 (2004).

[22] G. M. Preston, T. P. Carroll, W. B. Guggino, and P. Agre, Science **256**, 385 (1992).

[23] P. Agre, Agew. Chem. Int. Ed. **43**, 4278 (2004).

[24] R. Zardoya, Biol. Cell **97**, 397 (2005).

[25] M. Assentoft, B. R. Larsen, and N. MacAulay, Neurochem. Res. **40**, 2615 (2015).

[26] M. Amiry-Moghaddam and O. P. Ottersen, Nat. Rev. Neurosci. **4**, 991 (2003).

[27] M. C. Papadopoulos and A. S. Verkman, Pediatr. Nephrol. **22**, 778 (2007).

[28] X. Yao, N. Derugin, G. T. Manley, and A. S. Verkman, Neurosci. Lett. **584**, 368 (2015).

[29] M. C. Papadopoulos and A. S. Verkman, Nat. Rev. Neurosci. **14**, 265 (2013).

[30] M. C. Papadopoulos and A. S. Verkman, J. Biol. Chem. **280**, 13906 (2005).

[31] J. Kume-Kick, T. Mazel, I. Vorisek, S. Hrabetova, L. Tao and C. Nicholson, J. Physiol. **542**, 515 (2002).

[32] C. Nicholson, P. Kamali-Zare, and L. Tao, Comput. Visual Sci. **14**, 309 (2011).

[33] J. A. Sethian, J. Diff. Geom. **31**, 131 (1990).

[34] J. A. Sethian, *Level Set Methods* (Cambridge University Press, Cambridge, UK, 1996).

[35] L. Reuss, *Encyclopedia of Life Sciences* (John Wiley & Sons, Chichester, 2008).

[36] C. Bringedal, I. Berre, I. S. Pop, and F. A. Radu, Transp. Porous Med. **114**, 371 (2016).

[37] T. F. Weiss, *Cellular Biophysics* (MIT Press, Cambridge, MA, 1996).

[38] M. Jaeger, M. Carin, M. Medale, and G. Tryggvason, Biophys. J. **77**, 1257 (1999).

[39] A. Bensoussan, J. L. Lions, and G. Papanicolaou, *Asymptotic Analysis of Periodic Structures* (North-Holland, Amsterdam, 1978).

[40] U. Hornung, *Homogenization and Porous Media* (Springer, New York, 1996).

[41] H. G. Othmer, J. Math. Biol. **17**, 351 (1983).

[42] C. Sample and S. Y. Shvartsman, Proc. Natl. Acad. Sci. USA **107**, 10092 (2010).

[43] E. R. Higgins, P. Goel, J. L. Puglisi, D. M. Bers, M. Cannell, and J. Sneyd, J. Theor. Biol. **247**, 623 (2007).

[44] P. M. Kekenes-Huskey, T. Liao, A. K. Gillette, J. E. Hake, Y. Zhang, A. P. Michailova, A. D. McCulloch, and J. A. McCammon, Biophys J. **105**, 2130 (2013).

[45] M. A. Peter and M. Böhm, Math. Methods Appl. Sci. **31**, 1257 (2008).

[46] M. Panfilov, *Macroscale Models of Flow Through Highly Heterogeneous Porous Media* (Kluwer Academic, Dordrecht, The Netherlands, 2008).

[47] T. van Noorden, Multiscale Model. Simul. **7**, 1220 (2009).

[48] D. Gilbarg and N. S. Trudinger, *Elliptic Partial Differential Equations of Second Order* (Springer, New York, 2015).

[49] N. Ray, T. van Noorden, F. Frank, and P. Knabner, Transp. Porous Media **95**, 669 (2012).

[50] M. Zelenina and H. Brismar, Eur. Biophys. J. **29**, 165 (2000).

[51] E. Gunnarson, G. Axehult, G. Baturina, S. Zelenin, M. Zeleninaa, and A. Aperia, Neuroscience **136**, 105 (2005).

[52] A. Ern and J. L. Guermond, *Theory and Practice of Finite Elements* (Springer, New York, 2004).

[53] I. Klatzo, *Evolution of Brain Edema Concepts* (Springer, Berlin, 1994), pp. 3–6.

[54] D. Liang, S. Bhatta, V. Gerzanich, and J. M. Simard, Neurosurg. Focus **22**, 1 (2007).

[55] L. Dmytrenko, M. Cicanic, M. Anderova, I. Vorisek, O. P. Ottersen, E. Sykova, and L. Vargova, PLoS ONE **8**, e68044 (2013).

[56] E. I. Gusev and V. I. Skvortsova VI, *Brain Ischemia* (Kluwer Academic/Plenum, New York, 2003).

[57] N. N. Haj-Yasein, C. E. Bugge, V. Jensen, I. Ostby, O. P. Ottersen, Ø. Hvalby, and E. A. Nagelhus, Brain Struct. Funct. **220**, 2469 (2015).

[58] G. T. Manley *et al.*, Nat. Med. **6**, 159 (2000).

[59] E. Syková and C. Nicholson, Physiol. Rev. **88**, 1277 (2008).

[60] L. Yang, J. C. Effler, B. L. Kutscher, S. E. Sullivan, D. N. Robinson, and P. A. Iglesias, BMC Syst. Biol. **2**, 68 (2008).

[61] L. Wang, Y. Chen, X. Pan, X. Hong, and D. Xia, J. Neurosci. Methods **188**, 316 (2010).

[62] A. Tao, L. Tao, and C. Nicholson, J. Theor. Biol. **234**, 525 (2005).

[63] X. Yao, S. Hrabětová, C. Nicholson, and G. T. Manley, J. Neurosci. **28**, 5460 (2008).

[64] I. Ostby *et al.*, PLoS Comput. Biol. **5**, e1000272 (2009).

[65] P. Kamali-Zare, Ph.D. thesis, Royal Institute of Technology (KTH), 2010.

[66] A. G. Cherstvy and R. Metzler, J. Stat. Mech.: Theor. Exp. (2015) P05010.

[67] D. S. Novikov, J. H. Jensen, J. A. Helpern, and E. Fieremans, Proc. Natl. Acad. Sci. USA **111**, 5088 (2014).

[68] D. C. Van Essen, S. M. Smith, D. M. Barch, T. E. J. Behrens, E. Yacoub, K. Ugurbil, for the WU-Minn HCP Consortium, Neuroimage **80**, 62 (2013).

[69] M. J. Knight, B. McCann, R. A. Kauppinen, and E. J. Coulthard, Front. Aging Neurosci. **8**, 139 (2016).

[70] D. S. Novikov, E. Fieremans, J. H. Jensen, and J. A. Helpern, Nat. Phys. **7**, 508 (2011).